Journal of Alloys and Compounds 583 (2014) 70–78

Contents lists available at ScienceDirect

Journal of Alloys and Compounds

journal homepage: www.elsevier.com/locate/jalcom

Structural and elastic properties of defect chalcopyrite $HgGa_2S_4$ under high pressure

O. Gomis [a,*], D. Santamaría-Pérez [b,c], R. Vilaplana [a], R. Luna [a], J.A. Sans [d], F.J. Manjón [d], D. Errandonea [b], E. Pérez-González [e], P. Rodríguez-Hernández [e], A. Muñoz [e], I.M. Tiginyanu [f], V.V. Ursaki [f]

[a] Centro de Tecnologías Físicas: Acústica, Materiales y Astrofísica, MALTA Consolider Team, Universitat Politècnica de València, 46022 València, Spain
[b] Departamento de Física Aplicada-ICMUV, MALTA Consolider Team, Universitat de València, Edificio de Investigación, C/Dr. Moliner 50, Burjassot, 46100 València, Spain
[c] Departamento de Química Física I, Universidad Complutense de Madrid, MALTA Consolider Team, Avenida Complutense s/n, 28040 Madrid, Spain
[d] Instituto de Diseño para la Fabricación y Producción Automatizada, MALTA Consolider Team, Universitat Politècnica de València, 46022 València, Spain
[e] Departamento de Física Fundamental II, Instituto de Materiales y Nanotecnología, MALTA Consolider Team, Universidad de La Laguna, 38205 Tenerife, Spain
[f] Institute of Applied Physics, Academy of Sciences of Moldova, 2028 Chisinau, Moldovia

ARTICLE INFO

Article history:
Received 28 May 2013
Received in revised form 9 August 2013
Accepted 19 August 2013
Available online 29 August 2013

Keywords:
Semiconductors
Equation of state
Elasticity
Mechanical properties
High-pressure
X-ray diffraction

ABSTRACT

In this work, we focus on the study of the structural and elastic properties of mercury digallium sulfide ($HgGa_2S_4$) at high pressures. This compound belongs to the family of AB_2X_4 ordered-vacancy compounds and exhibits a tetragonal defect chalcopyrite structure. X-ray diffraction measurements at room temperature have been performed under compression up to 15.1 GPa in a diamond anvil cell. Our measurements have been complemented and compared with *ab initio* total energy calculations. The axial compressibility and the equation of state of the low-pressure phase of $HgGa_2S_4$ have been experimentally and theoretically determined and compared to other related ordered-vacancy compounds. The pressure dependence of the theoretical cation–anion and vacancy-anion distances and compressibilities in $HgGa_2S_4$ are reported and discussed in comparison to other related ordered-vacancy compounds. Finally, the pressure dependence of the theoretical elastic constants and elastic moduli of $HgGa_2S_4$ has been studied. Our calculations indicate that the low-pressure phase of $HgGa_2S_4$ becomes mechanically unstable above 13.8 GPa.

1. Introduction

Mercury digallium sulfide ($HgGa_2S_4$) is a tetrahedrally-coordinated semiconductor of the $A^{II}B^{III}_2X^{VI}_4$ family which crystallizes at ambient conditions in the tetragonal defect chalcopyrite (DC) structure (S.G. I-4, No. 82, $Z = 2$) [1–3]. The unbalanced number of cations (A and B) and anions (X) in tetrahedrally-coordinated $A^{II}B^{III}_2X^{VI}_4$ semiconductors results in inequivalent tetrahedrally-coordinated A and B cations (located in different Wyckoff sites) and in the occupation of a cation site by a vacancy in an ordered and stoichiometric fashion. For this reason, these semiconductors are classified as ordered-vacancy compounds (OVCs). The lack of cubic symmetry and the rather strong anisotropy make OVCs suitable for many technological applications [4–7].

$HgGa_2S_4$ is of considerable interest because it combines nonlinear optical properties in the mid-infrared range, high non-linear susceptibility coefficients, birefringence, and a wide transparency range from 0.5 to 13 μm [8–11]. This compound can be used for frequency doubling, optical parametric oscillator, and optical parametric amplifier in the wavelength range from 1.0 to 10 μm because the high values of laser damage threshold and conversion efficiency are combined with a suitable thermal conductivity and high specific heat capacity [11,12]. In fact, the combined properties of $HgGa_2S_4$ crystals make this compound to potentially occupy a leading position among the crystals used in non-linear optical devices [11].

Several high-pressure (HP) studies on $A^{II}B^{III}_2X^{VI}_4$ compounds have been carried out in the last years [13–34]. In particular, HP X-ray diffraction (XRD) measurements have been performed on $CdGa_2Se_4$ [18], $MnGa_2Se_4$ [24], $ZnGa_2Se_4$ [26], $CdGa_2S_4$ [26], $CdAl_2Se_4$ [25], $HgAl_2Se_4$ [27], $CdAl_2S_4$ [27], and $HgGa_2Se_4$ [32,33]. However, to the best of our knowledge, there is no study published on the structural and elastic properties of $HgGa_2S_4$ under pressure. We present here HP XRD measurements up to 15.1 GPa and *ab initio* total energy calculations in DC-$HgGa_2S_4$ in order to study the structural properties of the low-pressure phase of $HgGa_2S_4$. In particular, its equation of state (EOS) and the axial compressibilities are reported. We have also carried out calculations of the elastic prop-

* Corresponding author. Address: Departamento de Física Aplicada, Escuela Politécnica Superior de Alcoy, Universitat Politècnica de València, Placeta Ferrandiz Carbonell 2, 03802 Alcoy (Alicante), Spain. Tel.: +34 96 652 8426; fax: +34 96 652 8485.
E-mail address: osgohi@fis.upv.es (O. Gomis).

0925-8388/$ - see front matter © 2013 Elsevier B.V. All rights reserved.
http://dx.doi.org/10.1016/j.jallcom.2013.08.123

erties of DC-$HgGa_2S_4$ and have studied its mechanical stability under pressure.

2. Experimental section

Single crystals of DC-$HgGa_2S_4$ have been grown from its constituents HgS and Ga_2S_3 by chemical vapor transport method using iodine as a transport agent [35]. The as-grown crystals of uniform light-yellow color represent triangular prisms with mirror surfaces. Chemical and structural analyses have shown the stoichiometric composition of the crystals and no spurious phases have been observed [3]. The samples used in this study were already characterized at room pressure (RP) by XRD in the 2θ range of 5–85° collected using a DRON-R4M diffractometer with Cu Kα radiation [3] and by Raman spectroscopy [34] confirming that our sample has a DC-type structure.

HP angle-dispersive powder XRD experiments at room temperature have been performed in a modified diamond anvil cell (DAC) with an Oxford Xcalibur diffractometer. The same setup has been recently used to successfully characterize the HP behavior of several sulfides and selenides [33,36,37]. The DAC used for the experiments has an angular access of $2\theta = 25°$ and diamond anvils with 500 μm of culet size. The powder samples were placed in the 150 μm-diameter hole of a stainless-steel gasket preindented to a thickness of 50 μm. A 4:1 methanol–ethanol mixture was used as quasi-hydrostatic pressure-transmitting medium (PTM) [38,39]. Pressure was determined by the ruby fluorescence method [40] and in our experiment it has been limited to 15.1 GPa to avoid the influence of deviatoric stresses and of precursor effects [41] associated to the phase transitions observed in this compound [34] and in other $A^{II}B_2^{III}X_4^{VI}$ OVCs between 15 and 23 GPa [18,24–27,32]. X-ray beam collimated to a diameter of 300 μm from Mo Kα radiation ($\lambda = 0.7107$ Å) allowed to collect XRD patterns on a 135 mm Atlas CCD detector placed at 110 mm from the sample. A small phi rotation from −2 to 2° (width 2°) was used for the images collected on the Atlas CCD. In this particular experiment, the CCD was placed in two different positions, at −4 and 4°. Taking into account this and the aforementioned phi rotation and width, the total amount of frames was four. The total exposure time per image was 10 min, being the approximate data collection time 40 min. Dark images were previously collected with a similar exposure time. The CrysAlis software [42] was used for data collection and preliminary data reduction. The observed intensities were integrated as a function of 2θ in order to give conventional, one-dimensional diffraction profiles. No smoothing procedure was used in the integration procedure. The indexing and refinement of the powder diffraction patterns were performed using the CHEKCELL [43], POWDERCELL [44], and GSAS [45,46] program packages.

3. Theoretical calculation details

Ab initio total energy calculations have been carried out for DC-$HgGa_2S_4$ within the density functional theory (DFT) using the plane-wave method and the pseudopotential theory with the Vienna *ab initio* simulation package (VASP) [47]. The set of plane waves employed extended up to a kinetic energy cutoff of 370 eV. The generalized gradient approximation (GGA) has been used for the description of the exchange–correlation energy with the PBEsol exchange–correlation prescription [48]. We used dense special point grids appropriate to sample the Brillouin zone (BZ) when relaxing the structure at different volumes. Pressure, like other energy derivatives, is obtained at the same time from the stress tensor [49]. Additional details of total energy calculations in the DC structure of OVCs can be consulted in Ref. [29].

In order to study the mechanical properties of DC-$HgGa_2S_4$ by means of *ab initio* calculations we have calculated the elastic constants, which describe the mechanical properties of a material in the region of small deformations; i.e., where the stress–strain relations are still linear. The elastic constants can be obtained by computing the macroscopic stress for a small strain with the use of the stress theorem [50]. Alternatively, the macroscopic stress can be also calculated using density functional perturbation theory (DFPT) [51]. In this work, we have evaluated the elastic constants of DC-$HgGa_2S_4$ as implemented in the VASP code: the ground state and fully relaxed structures were strained in different directions according to their symmetry [52]. Total energy variations have been evaluated according to a Taylor expansion for the total energy with respect to the applied strain [53]. Due to this fact, it is important to check that the strain used in the calculations guarantees the harmonic behavior. This procedure allows the computation of the C_{ij} elastic constants in the Voigt notation where the number of independent elastic constants is reduced by crystalline symmetry [54]. The mechanical stability of the low-pressure phase of $HgGa_2S_4$ has been studied from a theoretical point of view using the generalized stability criteria.

4. Results and discussion

4.1. X-ray diffraction and structural properties

As already commented, $HgGa_2S_4$ crystallizes in the tetragonal defect chalcopyrite (DC) structure at room conditions [1–3]. Table 1 shows the crystallographic parameters of DC-$HgGa_2S_4$ at RP obtained from a Rietveld refinement of XRD data taken from Ref. [3]. Results for our samples are comparable to our theoretical calculations and to those of Refs. [1,2] (see Table 1).

Fig. 1 shows the XRD patterns of $HgGa_2S_4$ from RP to 15.1 GPa taken with the Xcalibur diffractometer. Those XRD patterns have been analyzed in the range $2\theta \leqslant 18.3°$ due to the presence of intense peaks of the stainless-steel gasket at higher angles. At the bottom of Fig. 1 we show in solid line the measured XRD pattern of our sample at RP along with the Miller indexes of the Bragg reflections for the DC phase. Vertical marks representing the positions of the Bragg reflections are also plotted. Diffractograms from RP to 15.1 GPa on upstroke could be indexed with the low-pressure tetragonal DC phase. The diffraction peaks only move to higher angles as pressure increases, thus indicating that compression causes a decrease of interplanar distances. In the angular region $2\theta \leqslant 18.3°$ the DC phase has nine Bragg peaks which allow obtaining the pressure evolution of the unit-cell parameters by means of a Le Bail refinement. Pressures, unit-cell parameters and volume for DC-$HgGa_2Se_4$ are listed in Table 2 along with the *R*-factors obtained from the Le Bail refinement. Broadening of the diffraction peaks, caused by the deterioration of the quasi-hydrostatic conditions of the experiment beyond 10 GPa, can be observed in Fig. 1[38,55]. In order to avoid the effects of deviatoric stresses on the quantitative study of the structural properties of DC-$HgGa_2S_4$, the axial compressibilities and the bulk modulus will be estimated using experimental data below 10 GPa because in this range the methanol–ethanol mixture maintains quasi-hydrostatic conditions [38].

Fig. 2 shows the pressure dependence of the lattice parameters for DC-$HgGa_2S_4$ from data obtained in XRD experiments (symbols) and from calculations (solid line). The experimental axial compressibilities for *a* and *c* axes at RP, defined as $\kappa_x = \frac{-1}{x}\frac{\partial x}{\partial P}$ and obtained by fitting of a Murnaghan EOS [56], are $\kappa_a = 7.6(6) \times 10^{-3}$ GPa^{-1} and $\kappa_c = 5.3(8) \times 10^{-3}$ GPa^{-1}. Our experiments show an anisotropy in the axial compression being the *a* axis more compressible than the *c* one. This result agrees with our theoretical results $\kappa_a = 8.9 \times 10^{-3}$ GPa^{-1} and $\kappa_c = 7.0 \times 10^{-3}$ GPa^{-1} and with previous results for other AB_2X_4 OVCs [18,24,26,27,32,33].

Fig. 3 shows the pressure dependence of the volume of the DC phase in $HgGa_2S_4$. EOS parameters of $HgGa_2S_4$ were determined by a least-squares fit of second order Birch–Murnaghan (BM2) and third-order Birch–Murnaghan (BM3) EOSs [57] to the experimental volume data. Weights derived from the experimental uncertainties in both pressure and volume were assigned to each data point in both fits. The fits were carried out with the v5.2 of the EoSFit software [58]. The RP values of the volume V_0 and bulk modulus B_0 obtained from fitting experimental data below 10 GPa with a BM2 EOS are summarized in Table 3. In the case of the BM2 EOS the first-pressure derivative of the bulk modulus B_0' is fixed to 4. The obtained value for the weighted chi-squared, χ_w^2, in the BM2 EOS fit is 1.16. The EOS parameters obtained with the BM3 EOS fit

Table 1
Experimental and theoretically calculated lattice parameters and relative atomic positions of tetragonal DC-$HgGa_2S_4$ at RP. The Rietveld refinement carried out at RP has residuals R_p = 16.5%, and R_{wp} = 9.7%. Hg, Ga(1), Ga(2), and the vacancy are located at the 2*a* (0,0,0), 2*b* (0,0,0.5), 2*c* (0,0.5,0.25), and 2*d* (0,0.5,0.75) Wyckoff positions, respectively. The relative atomic coordinates of the sulfur anion located at the 8*g* (*x*, *y*, *z*) Wyckoff position are given in the table.

	X-ray diffraction[a]	*Ab initio* PBEsol[b]	X-ray diffraction[c]	X-ray diffraction[d]
a (Å)	5.5095(3)	5.5125	5.507	5.5106(1)
c (Å)	10.2308(6)	10.2015	10.23	10.2392(2)
S site:	*x* = 0.272(1)	*x* = 0.2743	*x* = 0.275	*x* = 0.2718(3)
8*g*	*y* = 0.268(1)	*y* = 0.2665	*y* = 0.265	*y* = 0.2675(3)
	z = 0.1375(6)	*z* = 0.1390	*z* = 0.139	*z* = 0.1374(1)

[a] Obtained from experimental results of Ref. [3].
[b] Our calculations.
[c] Ref. [1].
[d] Ref. [2].

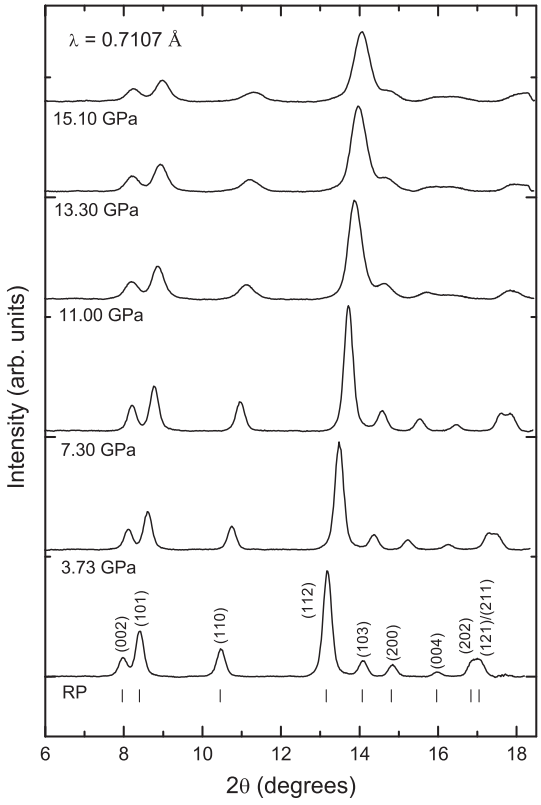

Fig. 1. Room temperature XRD patterns of $HgGa_2S_4$ at different pressures from RP up to 15.1 GPa. In all diagrams, the background was subtracted. In the XRD pattern at RP, Bragg reflections are indicated with vertical ticks.

Table 2
Experimental pressure (*P*), unit-cell parameters (*a*, *c*) and volume (*V*) of DC-$HgGa_2S_4$ with their standard deviations. The R_p and R_{wp} factors obtained from a Von Dreele-type Le Bail refinement are also given.

P (GPa)	Esd (*P*) (GPa)	*a* Å	Esd (*a*) (Å)	*c* Å	Esd (*c*) (Å)	*V* (Å^3)	Esd (*V*) Å^3	R_p (%)	R_{wp} (%)
0.00	0.00	5.506	0.001	10.219	0.003	309.80	0.21	7.6	18.1
0.03	0.01	5.505	0.001	10.217	0.003	309.61	0.20	7.2	18.2
0.68	0.01	5.477	0.001	10.186	0.003	305.52	0.20	11.9	18.4
1.20	0.01	5.460	0.001	10.162	0.002	302.90	0.17	8.2	17.4
1.35	0.01	5.449	0.001	10.157	0.002	301.57	0.17	8.0	17.4
2.04	0.01	5.425	0.001	10.128	0.002	298.01	0.17	7.7	16.9
2.20	0.01	5.422	0.001	10.114	0.004	297.30	0.23	9.7	16.4
2.75	0.01	5.400	0.001	10.096	0.002	294.39	0.17	7.5	17.9
3.73	0.01	5.364	0.001	10.048	0.002	289.13	0.17	7.1	17.0
3.95	0.01	5.359	0.001	10.052	0.002	288.68	0.17	8.0	17.4
4.67	0.01	5.339	0.001	10.021	0.002	285.67	0.16	7.8	18.1
5.30	0.01	5.318	0.001	9.999	0.002	282.73	0.16	8.5	18.6
5.74	0.01	5.311	0.001	9.990	0.003	281.83	0.19	10.5	18.1
6.05	0.01	5.297	0.001	9.975	0.002	279.85	0.16	6.1	15.8
6.62	0.01	5.278	0.001	9.962	0.002	277.48	0.16	8.8	18.1
6.80	0.01	5.276	0.001	9.958	0.003	277.15	0.19	12.7	20.0
7.30	0.01	5.257	0.001	9.948	0.002	274.94	0.16	8.0	17.5
8.20	0.01	5.238	0.001	9.920	0.003	272.13	0.19	11.6	17.8
11.00	0.02	5.168	0.001	9.878	0.004	263.86	0.21	10.8	17.9
13.30	0.02	5.129	0.001	9.840	0.004	258.82	0.21	10.6	18.8
15.10	0.02	5.089	0.001	9.818	0.005	254.24	0.23	11.7	20.5

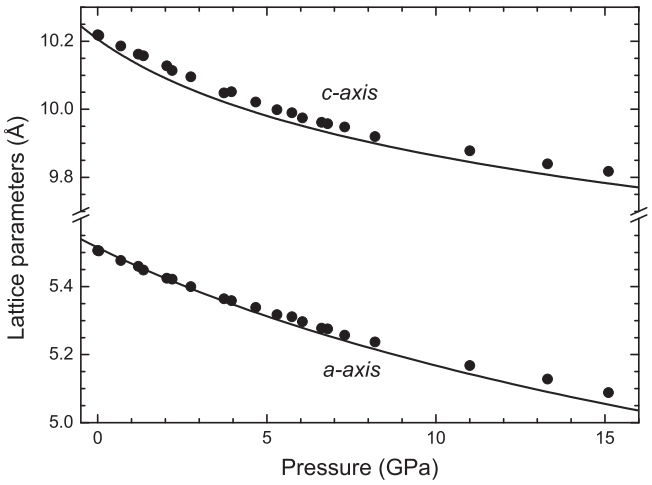

Fig. 2. Lattice parameters of the DC phase of $HgGa_2S_4$ as a function of pressure. Symbols refer to experimental data. Theoretical results are plotted with solid line.

are included in Table 3. In this case, the refinement of the B_0' parameter does not improve the fit of the data because the χ^2_w increases to a value of 1.25 and the standard deviations of V_0 and B_0 increase with respect to those obtained with the BM2 EOS, thus indicating that an expansion of the EOS to third order is not required to fit the data. These results show that the second-order equation of state is an adequate representation of the volume–pressure data of $HgGa_2S_4$.

In order to obtain a direct indication of the compressional behavior of DC-$HgGa_2S_4$ and of the quality of the EOS fit, the *P*–*V* data are transformed into *F*–*f* data where *F* is the normalized stress and *f* the finite strain [58]. For the Birch–Murnaghan EOS, based upon the Eulerian definition of finite strain f_E, the normalized pressure is defined as $F_E = P/(3f_E(1+2f_E)^{5/2})$ with the Eulerian strain defined as $f_E = [(V_0/V)^{2/3}-1]/2$ [58]. In a F_E–f_E plot, if the data points all lie on a horizontal line of constant F_E then $B_0' = 4$, and the data can be fitted with a BM2. If the data lie on an inclined straight line, the slope is equal to $3B_0(B_0'-4)/2$, and the data will be adequately described by a BM3 [58]. In both cases, the intercept on the vertical F_E axis is the value of B_0. The F_E–f_E plot for DC-$HgGa_2S_4$ is shown in Fig. 4 with the uncertainties in f_E and F_E. It is seen that a linear fit to experimental data (blue dashed line) gives a straight line almost parallel to the case when $B_0' = 4$ (solid red line). A value of B_0 = 48.5(7) GPa is obtained from the linear fit. The linear fit gives a small positive slope from which a $B_0' = 4.0(3)$ is obtained. These results show that the BM2 EOS is an adequate representation of the volume–pressure data of $HgGa_2S_4$ as has been previously found on the basis of statistical results from the EOS fits.

Theoretical data have been fitted with BM2 and BM3 EOSs and the results for the V_0, B_0 and B_0' parameters are included in Table 3. It can be observed that our experimental and theoretical results are in relatively good agreement. For comparison purposes, Table 4

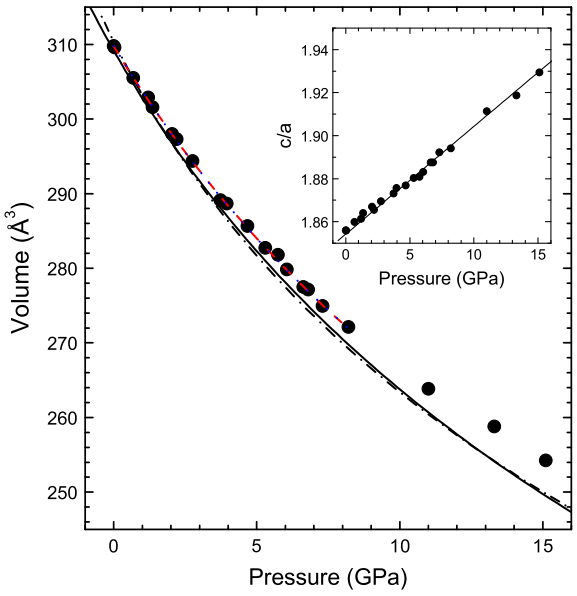

Fig. 3. Volume of the DC phase of $HgGa_2S_4$ as a function of pressure. Experimental data (symbols) and their fit with a BM2 (red dashed line) and a BM3 (blue dotted line) EOS are shown. The fit with a BM2 and BM3 EOS to theoretical data is shown with solid and dash-dotted lines, respectively. The inset shows the evolution of the c/a ratio of the DC phase as a function of pressure: experimental data (symbols), theoretical data (solid line). (For interpretation of the references to color in this figure legend, the reader is referred to the web version of this article.)

Table 3
Experimentally determined and calculated EOS for DC-$HgGa_2S_4$ at RP. Last column indicates the EOS type used (BM2 = Birch–Murnaghan of order 2, BM3 = Birch–Murnaghan of order 3).

	V_0 (Å^3)	B_0 (GPa)	B_0'	EOS type
Experiment	309.77(11)	48.4(3)	4 (fixed)	BM2
Experiment	309.80(14)	48.1(9)	4.1(3)	BM3
Calculation	309.8(2)	44.0(4)	4 (fixed)	BM2
Calculation	310.4(1)	40.8(1)	4.9 (1)	BM3

summarizes the B_0 and B_0' parameters obtained experimentally for several AB_2X_4 OVCs. Since both parameters are strongly correlated [59] and they may depend on the hydrostatic conditions of the experiments [32], care should be taken when comparing B_0 values. For that reason the PTM used during the experiment is also reported in Table 4. It can be observed that for DC-$HgGa_2S_4$ the experimental B_0 (48.4(3) GPa) obtained with the BM2 EOS is similar to that obtained in other OVCs.

Now we will study the evolution of the c/a ratio with pressure in DC-$HgGa_2S_4$ since the tetragonal distortion, $\delta = 2-c/a$, could give important information about the behavior of the sample on compression. Inset of Fig. 3 shows the experimental (symbols) and theoretical (solid line) pressure dependence of the c/a ratio vs. pressure. It can be observed that c/a increases with increasing pressure from 1.856 at RP to 1.929 at 15.1 GPa. Therefore, our results show that DC-$HgGa_2S_4$, like other DC compounds [18,24,26,27,31–33], tends to a more symmetrical structure on compression. Furthermore, the evolution of the experimental c/a ratio with pressure is also well reproduced by our calculations. It must be noted that the increase of the c/a ratio has been previously considered as a measure of cation-vacancy disorder [60,61]. However, since no cation-vacancy disorder is assumed in our calculations, the good agreement between our experimental and theoretical results suggests that the tetragonal distortion cannot be taken as a measure of the cation-vacancy disorder in the tetragonal DC structure at any pressure as previously thought [15].

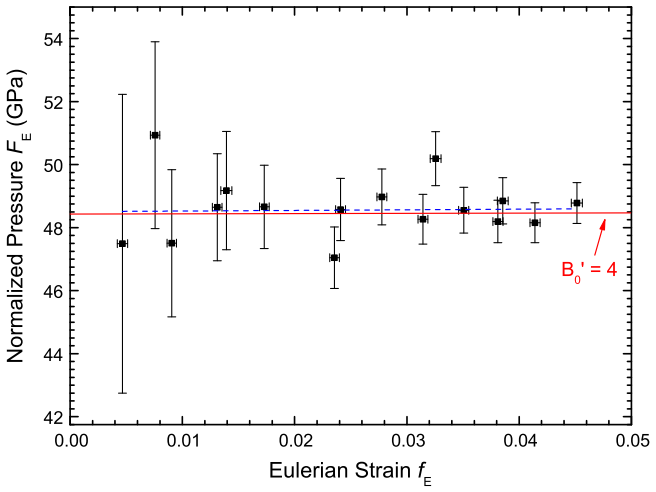

Fig. 4. Volume–pressure data of DC-$HgGa_2S_4$ displayed as a plot of the normalized pressure F_E against the Eulerian strain f_E. The blue dashed line is a linear fit to experimental F_E–f_E data. Solid red line represents the case of a BM2 EOS with $B_0' = 4$. (For interpretation of the references to color in this figure legend, the reader is referred to the web version of this article.)

It was also thought that information on the cation-vacancy disorder could be obtained from the study of the pressure dependence of the axial compressibilities κ_a and κ_c and their difference [24,33]. This information is shown for DC-$HgGa_2S_4$ in the top and low panels of Fig. 5 for XRD experiments and calculations, respectively. As can be seen, in both cases, the κ_a and κ_c compressibilities decrease with pressure as observed previously in other OVCs [24,33]. Furthermore, the κ_a–κ_c difference is positive at every pressure, but has a non-linear pressure dependence with a positive pressure coefficient at low pressures and a negative pressure coefficient at high pressures. The value of the κ_a–κ_c maximum for DC-$HgGa_2S_4$ is found at about 4 GPa. A similar evolution was found previously for DC-$MnGa_2Se_4$ and $HgGa_2Se_4$ [24,33]. In this respect, it was proposed that the change in tendency of the difference κ_a–κ_c with pressure was a sign of the onset of the transformation from the DC phase to a disordered structure (around 3 GPa in $MnGa_2Se_4$) [24]. This would imply that cation disorder is increasing with pressure above that pressure. However, our calculations show a maximum for κ_a–κ_c at a similar pressure than in experiment despite cation disorder is not considered in the calculations. Since we have obtained the same results now for DC-$HgGa_2S_4$ than previously for DC-$HgGa_2Se_4$ [33], we reaffirm that unfortunately the change of the pressure coefficient of κ_a–κ_c cannot be considered a sign of the onset of the cation disorder in the tetragonal DC structure of AB_2X_4 OVCs.

In order to understand better how the structure of DC-$HgGa_2S_4$ behaves under compression we show in Fig. 6 (a) the theoretical pressure dependence of the cation–anion and vacancy-anion distances in DC-$HgGa_2S_4$. A good agreement is found between the calculated and experimental distances at RP. The largest distance is that of Hg-S, the intermediate distances are those of Ga(1)-S and Ga(2)-S, and the shortest distance is that of vacancy-S. Hg-S, Ga(1)-S, and Ga(2)-S distances are much less compressible than the vacancy-S distance, despite the latter is the smallest one. The high compressibility of the vacancy-S distance is due to the weak repulsion between the separated electron distributions of S atoms surrounding the vacancy. Consequently, S atoms move towards the vacancy site at a faster rate than to the sites occupied by cations. These calculated results for DC-$HgGa_2S_4$ agree nicely with those calculated for DC-$HgGa_2Se_4$[33] and with those experimentally obtained for DC-$CdGa_2Se_4$ from XRD measurements [18]. For completeness, we show in Fig. 6 (b) the compressibility of the

Table 4
Experimental bulk modulus (B_0), and its pressure derivative (B_0') at RP for several OVCs. The case when the B_0' parameter was fixed to 4 in the EOS fit is indicated. The PTM used in the different experiments is also included. Last column indicates the EOS type used (M = Murnaghan, BM2 = Birch–Murnaghan of order 2, BM3 = Birch–Murnaghan of order 3).

Compound	B_0 (GPa)	B_0'	PTM	Reference	EOS type
$CdAl_2S_4$	44.6(1)	4 (fixed)	Methanol–ethanol	[27]	BM2
$CdAl_2Se_4$	52.1	4 (fixed)	Methanol–ethanol	[25]	BM2
$CdGa_2S_4$	64(2)	4.1(3)	Silicone oil	[26]	BM3
$CdGa_2Se_4$	41.5(2)	5(1)	Methanol–ethanol	[18]	M
$HgAl_2Se_4$	66(1.5)	4 (fixed)	Paraffin oil	[27]	BM2
$HgGa_2S_4$	48.4(3)	4 (fixed)	Methanol–ethanol	This work	BM2
	48.1(9)	4.1(3)			BM3
$HgGa_2Se_4$	53(9)	6(2)	MgO	[32]	BM3
	39(2)	5.2(4)	Methanol–ethanol	[33]	BM3
$MnGa_2Se_4$	44(2) [a]	3.8(4)[a]	Methanol–ethanol, neon, and silicone oil	[24]	M
$ZnGa_2Se_4$	47(2)	3.9(3)	Silicone oil	[26]	BM3

[a] B_0 and B_0' parameters were obtained in Ref. [24] by means of a single EOS fit to data from three different experiments using each one of the three PTM indicated in the table.

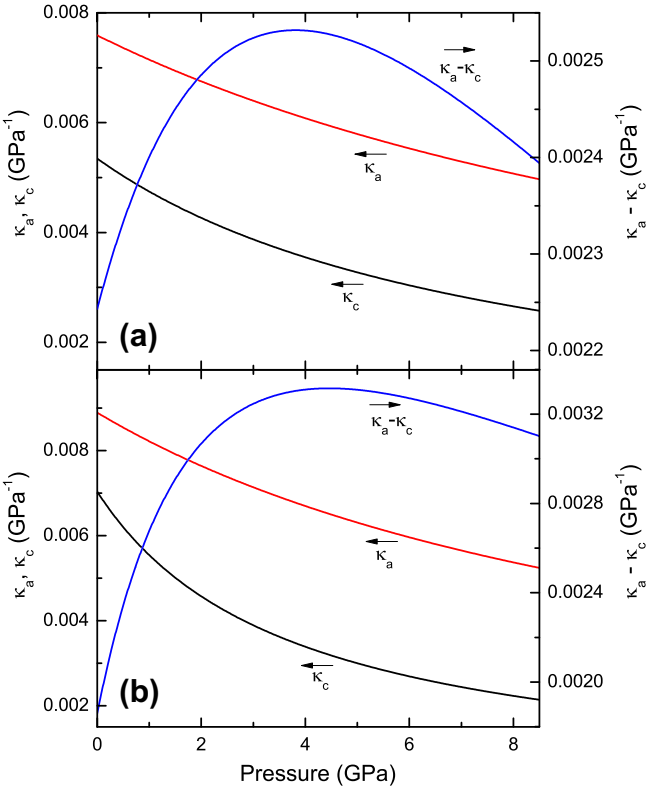

Fig. 5. Left side of panel: κ_a and κ_c vs. pressure. Right side of panel: (κ_a–κ_c) vs. pressure. Results correspond to: (a) XRD experiments, and (b) PBEsol calculations.

cation–anion and vacancy-anion internal distances for DC-$HgGa_2S_4$ as a function of pressure. The distance compressibility decreases following the sequence "vacancy-S > Hg-S > Ga(1)-S > Ga(2)-S". At HP, the compressibility of all cation–anion distances tends to approach to a similar value whilst the vacancy-S distance compressibility is still much larger. The calculated compressibility at RP for the average Ga-S, Hg-S, and vacancy-S distances are 2.7×10^{-3} - GPa^{-1}, 5.1×10^{-3} GPa^{-1}, and 21.4×10^{-3} GPa^{-1}; respectively.

4.2. Elastic properties

DC-$HgGa_2S_4$ belongs to the tetragonal Laue group TII and has seven independent second-order elastic constants named: C_{11}, C_{12}, C_{13}, C_{33}, C_{44}, C_{66}, and C_{16} [33]. The formulas for the calculation of the elastic moduli with the use of the elastic constants in the Laue group TII have not been derived analytically. This is due to the presence of the off-diagonal shear elastic constant C_{16} which is usually different from zero. However, it is possible to transform the seven components C_{ij} of the elastic tensor of a TII crystal into the six components C_{ij}' of the elastic tensor of a TI crystal, for which the formulas for the calculation of the elastic moduli are available. For that purpose one needs to make C_{16} equal to zero by means of a rotation around the Z axis through an angle given by [62,63]:

$$\phi_{\kappa,\gamma} = \frac{1}{4}\arctan\left(\frac{4C_{16}}{C_{11} - C_{12} - 2C_{66}}\right) \quad (1)$$

Eq. (1) gives two values for ϕ in the range $0 < \phi < |\pi/2|$ that correspond to ϕ_κ and ϕ_γ where $\phi_\gamma = \phi_\kappa + \pi/4$ [63,64]. For DC-$HgGa_2S_4$ at RP we obtain $\phi_\kappa = 3.72°$ and $\phi_\gamma = 48.72°$.

The equations used to obtain the six independent C_{ij}' elastic constants of a TI crystal as a function of the seven C_{ij} elastic constants of a TII crystal and the ϕ angle have been taken from Ref. [64]. Table 5 shows the set of seven elastic constants C_{ij} at RP obtained from our calculations together with the two sets of six C_{ij}' obtained for angles ϕ_κ and ϕ_γ. The results for DC-$HgGa_2S_4$ are compared to the theoretical results for DC-$HgGa_2Se_4$ [33], and for DC-$CdGa_2S_4$ and DC-$CdGa_2Se_4$ [65] (see Table 5). In general, values for C_{ij} are similar in the four compounds but are slightly larger for sulfides ($CdGa_2S_4$ and $HgGa_2S_4$) than for the corresponding selenides ($CdGa_2Se_4$ and $HgGa_2Se_4$).

With the set of six C_{ij}' elastic constants for DC-$HgGa_2S_4$, the bulk (B), and shear (G) moduli for the tetragonal Laue group TI in the Reuss [66], Voigt [67], and Hill [68] approximations, labeled with subscripts R, V, and H, respectively, have been calculated by using the Eqs. (2)–(7) given in Ref. [33] which were already used to calculate the elastic moduli for DC-$HgGa_2Se_4$ (see Table 5). In the Reuss (Voigt) approximations, uniform stress (strain) is assumed throughout the polycrystal [66,67]. Hill has shown that the Voigt and Reuss averages are limits and suggested that the actual effective B and G elastic moduli can be approximated by the arithmetic mean of the two bounds [68]. The Young (E) modulus and the Poisson's ratio (ν) are calculated by the Eqs. (8) and (9) given in Ref. [33]. Table 5 summarizes the obtained values of B, G, E, and ν for DC-$HgGa_2S_4$ at RP. It is found that DC-$HgGa_2S_4$ is more resistive to volume compression than to shear ($B > G$). Note that we have obtained a value for the bulk modulus in the Hill approximation of $B_H = 45.7$ GPa which is in very good agreement with the value of $B_0 = 48.4(3)$ GPa obtained from our XRD measurements via a second order Birch–Murnaghan EOS fit. This result gives us confidence about the correctness of our elastic constants calculations.

With the values of the seven calculated C_{ij} at RP reported in Ref. [65] for Cd-based compounds, we have obtained the six C_{ij}' at RP and the corresponding elastic moduli for comparison with Hg-based compounds (see Table 5). We must note that for DC-$CdGa_2$-

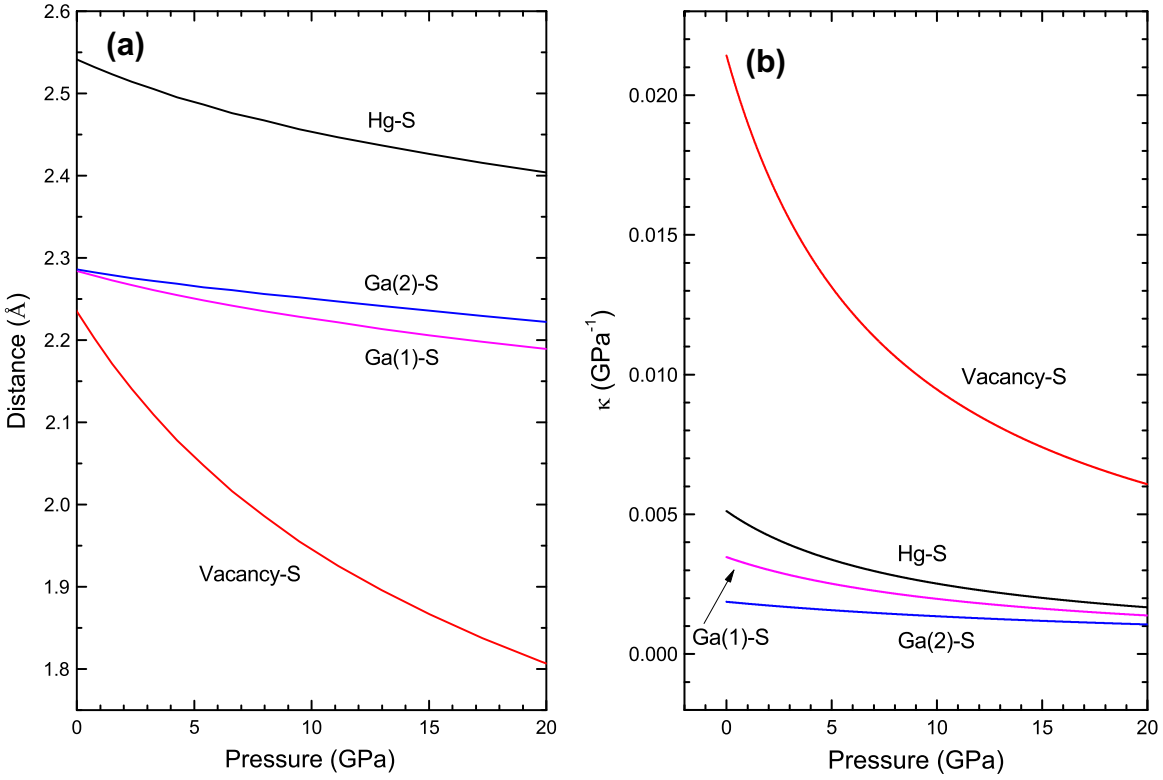

Fig. 6. (a) Calculated cation–anion and vacancy-anion distances, and (b) distance compressibilities as a function of pressure for DC-$HgGa_2S_4$.

Table 5
Seven C_{ij} and six C'_{ij} ($C'_{16}=0$) calculated elastic constants (in GPa) for DC-$HgGa_2S_4$ at RP. The elastic moduli B, G, and E (in GPa) and Poisson's ratio (v) are given in the Voigt, Reuss and Hill approximations, labeled respectively with subscripts V, R, and H. The B/G ratio and the shear anisotropy factor (A) are also included. The axial compressibilities κ_a and κ_c obtained from the elastic constants calculations are also given. Calculated data for DC-$HgGa_2Se_4$ [33], DC-$CdGa_2Se_4$ and DC-$CdGa_2S_4$ are also added [65] for comparison.

	DC-$HgGa_2S_4$	DC-$HgGa_2Se_4$	DC-$CdGa_2S_4$	DC-$CdGa_2Se_4$
C_{11}	65.6[a]	54.2[b]	61.8[c]	52.5[c]
C_{12}	32.5[a]	24.3[b]	24.7[c]	20.4[c]
C_{13}	38.0[a]	31.2[b]	35.7 [c]	38.8 [c]
C_{33}	63.4[a]	55.5[b]	50.0 [c]	60.0 [c]
C_{44}	35.6[a]	29.9[b]	33.9 [c]	31.6 [c]
C_{66}	31.6[a]	26.2[b]	27.0[c]	16.0[c]
C_{16}	−2.0[a]	−0.3[b]	−2.7 [c]	−1.9 [c]
C'_{11}	65.3[d], 80.9[e]	54.2[f], 65.5[g]	61.0[h,i], 71.0[h,j]	50.6[h,k], 54.3[hl],
C'_{12}	32.8[d], 17.2[e]	24.3[f], 13.0[g]	25.5[h,i], 15.4[h,j]	22.3[h,k], 18.6[h,l]
C'_{13}	38.0[d], 38.0[e]	31.2[f], 31.2[g]	35.7[h,i], 35.7[h,j]	38.8[h,k], 38.8[h,l]
C'_{33}	63.4[d], 63.4[e]	55.5[f], 55.5[g]	50.0[h,i], 50.0[h,j]	60.0[h,k], 60.0[h,l]
C'_{44}	35.6[d], 35.6[e]	29.9[f], 29.9[g]	33.9[h,i], 33.9[h,j]	31.6[h,k], 31.6[h,l]
C'_{66}	31.9[d], 16.3[e]	26.2[f], 14.9[g]	27.8[h,i], 17.7[h,j]	17.9[h,k], 14.1[h,l]
B_V, B_R, B_H	45.7, 45.7, 45.7	37.5, 37.2, 37.4	58.4[c], 40.6[h], 40.6[h], 40.6[h]	36.1[c], 40.1[h], 36.1[h], 38.1[h]
G_V, G_R, G_H	26.3, 21.6, 24.0	22.3, 18.8, 20.6	24.1[h], 17.3[h], 20.7[h]	20.3[h], 13.6[h], 16.9[h]
E_V, E_R, E_H	66.2, 56.0, 61.2	55.9, 48.4, 52.2	60.4[h], 45.5[h], 53.1[h]	52.1[h], 36.3[h], 44.3[h]
v_V, v_R, v_H	0.26, 0.30, 0.28	0.25, 0.28, 0.27	0.25[h], 0.31[h], 0.28[h]	0.28[h], 0.33[h], 0.31[h]
B_V/G_V, B_R/G_R, B_H/G_H	1.74, 2.11, 1.91	1.68, 1.98, 1.81	1.68[h], 2.35[h], 1.96[h]	1.98[h], 2.66[h], 2.25[h]
A	1.96[d], 0.51[e]	1.75[f], 0.57[g]	1.57[h,i], 0.64[h,j]	1.27[h,k], 0.79[h,l]
κ_a, κ_c (10^{-3} GPa^{-1})	7.6, 6.6	10.1, 6.7	8.1[h], 8.5[h]	15.6[h], −3.5[h]

[a] Our calculations.
[b] Data taken from Ref. [33].
[c] Data taken from Ref. [65].
[d,e] Rotation angle of $\phi_\kappa = 3.72°$ and $\phi_\gamma = 48.72°$, respectively.
[f,g] Rotation angle of $\phi_\kappa = 0.76°$ and $\phi_\gamma = 45.76°$, respectively.
[h] Obtained after the elastic constants reported in Ref. [65].
[i,j] Rotation angle of $\phi_\kappa = 8.20°$ and $\phi_\gamma = 53.20°$, respectively.
[k,l] Rotation angle of $\phi_\kappa = 22.27°$ and $\phi_\gamma = 67.27°$, respectively.

S_4 we obtain a value of the bulk modulus of 40.6 GPa instead of the value of 58.4 GPa reported by the authors.

Table 5 also includes the values of the ratio between the bulk and shear modulus, B/G, and the shear anisotropy factor A. The $B/$

G ratio is a simple relationship given by Pugh [69], empirically linking the plastic properties of a material with its elastic moduli. According to the Pugh criterion a high B/G ratio is associated with ductility, whereas a low ratio corresponds to brittleness. The critical value for the B/G ratio is around 1.75, which separates ductile and brittle materials. In our particular case, we found a value of $B/G = 1.91$ in the Hill approximation indicating that the material should be ductile but close to the limit of ductility at RP. Therefore, experimental measurements are needed to determine the plastic behavior of $HgGa_2S_4$ in practice. The elastic anisotropy of crystals is of importance for both engineering science and crystal physics since it is highly correlated to the possibility of inducing microcraks in the materials [70]. This anisotropy is quantified in our DC sample with the shear anisotropy factor A that for our tetragonal cell is defined as $A = 2C_{66}/(C_{11}-C_{12})$ [71]. If A is equal to 1, no anisotropy exists. On the other hand, the more this parameter differs from 1, the more elastically anisotropic is the crystalline structure. In our particular case, $A = 1.96$ and 0.51 for angles ϕ_κ and ϕ_γ, respectively. These values are rather different from 1 and evidence the anisotropy of our tetragonal cell at RP. Note that the anisotropy factors obtained for the two possible rotation angles follow the relation $0.51 = 1/1.96$, which is a direct consequence of the $\pi/4$ rotation around the z axis ($\phi_\gamma = \phi_\kappa + \pi/4$). We have also obtained the axial compressibilities κ_a and κ_c from our elastic constants calculations by using the Eq. (10) of Ref. [33]. Table 5 includes the values for κ_a and κ_c obtained at RP which are in good agreement with those obtained experimentally. Again, this result gives us confidence about the correctness of our elastic constants calculations.

We have also obtained the values of the B/G ratio, A factor, and κ_a and κ_c axial compressibilities for DC-$CdGa_2S_4$ and DC-$CdGa_2Se_4$ which are included in Table 5. We have found that the κ_a and κ_c axial compressibilities for the two Cd-based compounds obtained from C_{ij} data of Ref. [65] are not in good agreement with experimental values for κ_a and κ_c. The experimental κ_a and κ_c for DC-$CdGa_2S_4$ estimated from Ref. [26] are $\kappa_a = 5.9(8) \times 10^{-3}$ GPa^{-1} and $\kappa_c = 4.5(7) \times 10^{-3}$ GPa^{-1}. For the case of DC-$CdGa_2Se_4$, the experimental κ_a and κ_c estimated from Ref. [18] are $\kappa_a = 12.5(9)$ - $\times 10^{-3}$ GPa^{-1} and $\kappa_c = 8.3(6) \times 10^{-3}$ GPa^{-1}. The major discrepancy between theoretical and experimental values for κ_a and κ_c in DC-$CdGa_2Se_4$ is that theoretical κ_c has an unusual negative value of -3.5×10^{-3} GPa^{-1} unlike the positive experimental one. In the case of DC-$CdGa_2S_4$, the theoretical κ_a/κ_c ratio is smaller than 1, unlike the experimental κ_a/κ_c ratio which shows that the a axis is more compressible than the c one, as it is observed experimentally in all studied OVCs and in our calculations. These discrepancies indicate that more accurate calculations for the elastic constants of DC-$CdGa_2S_4$ and DC-$CdGa_2Se_4$ are needed.

In the following, we are going to study the mechanical stability of DC-$HgGa_2S_4$ at HP. For that purpose, we will analyze the pressure dependence of the elastic constants. Fig. 7 (a) shows the evolution of the seven calculated C_{ij} of DC-$HgGa_2S_4$ with pressure which could be useful for comparison to future experimental measurements of the elastic constants of DC-$HgGa_2S_4$ under pressure. It can be seen that the C_{11}, C_{12}, C_{13}, C_{33}, and C_{66} elastic constants increase monotonically as pressure increases. The C_{44} elastic constant increases up to a value of 9 GPa and above that pressure it decreases as pressure increases. Finally, the C_{16} elastic constant remains small in all the studied pressure range. In summary, the evolution of the seven C_{ij} with pressure for $HgGa_2S_4$ is similar to that found in $HgGa_2Se_4$ [33].

The study of the mechanical stability of a crystal under pressure requires the generalization of the Born–Huang stability criteria to the case when an external load is applied. In this way, the generalized stability criteria are obtained. For a detailed explanation of how these generalized stability criteria are deduced, we refer the reader to Ref. [72]. In practice, these criteria for tetragonal crystals

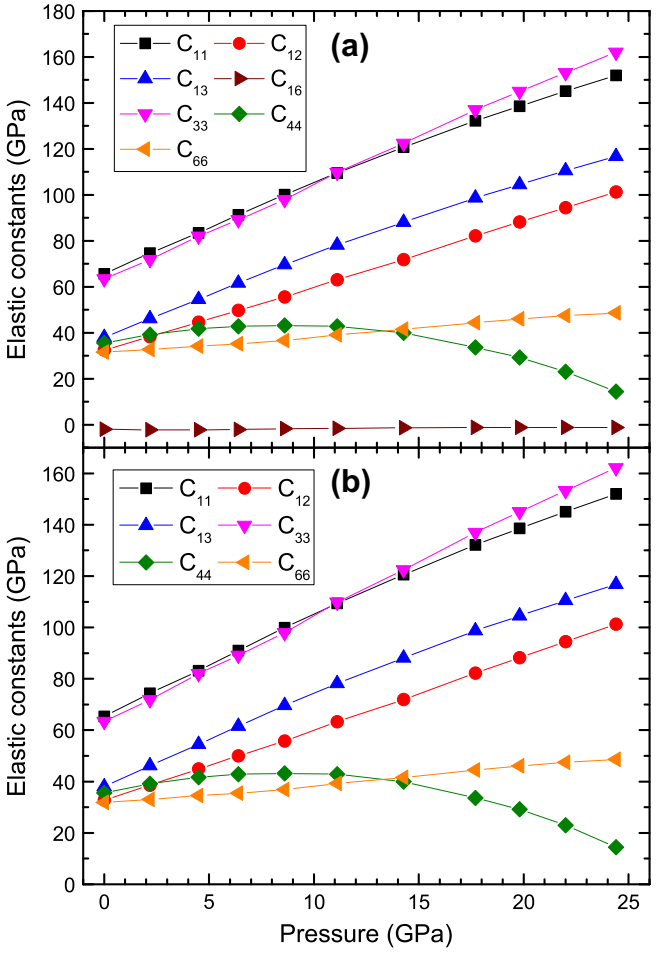

Fig. 7. Pressure dependence of the theoretical elastic constants of DC-$HgGa_2S_4$: (a) Seven C_{ij} elastic constants and (b) Six C'_{ij} elastic constants. Solid lines connecting the calculated data points are guides to the eyes.

with six elastic constants are given by the following conditions [33,72]:

$$C_{11} - P > 0, \tag{2}$$

$$C_{44} - P > 0, \tag{3}$$

$$C_{66} - P > 0, \tag{4}$$

$$C_{11} - C_{12} - 2P > 0 \tag{5}$$

$$(C_{33} - P)(C_{11} + C_{12}) - 2(C_{13} + P)^2 > 0 \tag{6}$$

All the above criteria are satisfied for DC-$HgGa_2S_4$ at RP, thus this tetragonal crystal is mechanically stable at RP, as expected. Fig. 7 (b) shows the pressure dependence of the six elastic constants for the case of $\phi_\kappa = 3.72°$ in order check whether DC-$HgGa_2S_4$ satisfies Eqs. (2)–(6) at HP. It can be observed that Eq. (6) is violated at a pressure of 13.8 GPa, Eq. (3) is violated at a pressure of 22.1 GPa, and Eq. (5) is violated at a pressure of 25.3 GPa. We highlight the fact that the pressures at which Eqs. (6), (3), and (5) are not satisfied are the same for both ϕ_κ and ϕ_γ transformations. Therefore, the study of the mechanical stability of DC-$HgGa_2S_4$ suggests that the tetragonal phase becomes mechanically unstable above a pressure of 13.8 GPa. This pressure is consistent with the pressure at which dark linear defects are observed. These defects are precursors of a phase transition of DC-$HgGa_2S_4$ to a disordered structure above 18 GPa and to a Raman-inactive phase above 23 GPa [34].

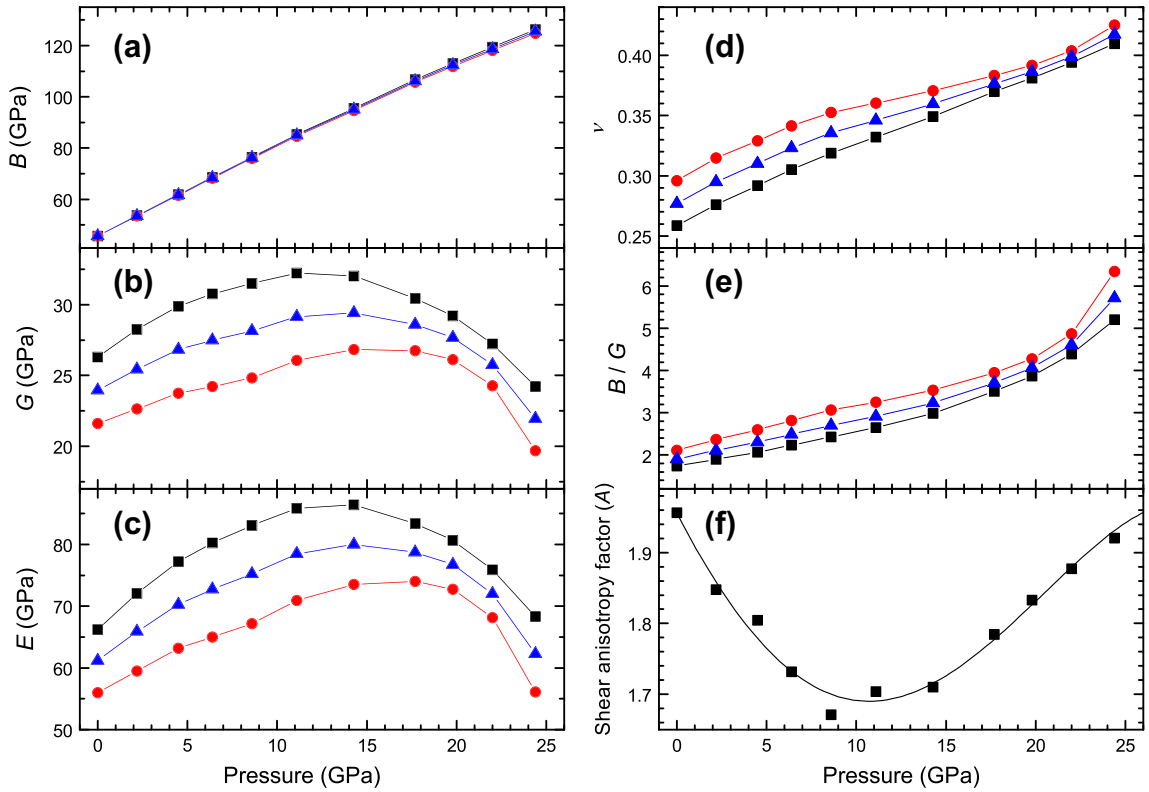

Fig. 8. Pressure dependence of (a) B, (b) G, (c) E, (d) ν, (e) B/G, and (f) A. Squares, circles, and triangles refer to the Voigt, Reuss, and Hill approximations; respectively. Data for the A anisotropy factor are shown for $\phi_\kappa = 3.72°$. Solid lines connecting the calculated data points are guides to the eyes in panels (a) to (e). Solid line in panel (f) represents the behavior of A with pressure.

To conclude, we report in Fig. 8 and discuss the pressure dependence of the B, G and E elastic moduli, the ν Poisson's ratio, the B/G ratio and the A factor. It can be observed that the bulk modulus increases as pressure increases reaching a value of $B_H = 93.9$ GPa at 14 GPa. The shear modulus increases with pressure reaching a maximum value of $G_H = 29.3$ GPa at 14.6 GPa and above that pressure it decreases as pressure increases. In the case of the Young modulus it increases with pressure reaching a maximum value of $E_H = 80.0$ GPa at 15.7 GPa and above that pressure it decreases as pressure increases. The Poisson's ratio and the B/G ratio increase as pressure increases reaching a value $\nu_H = 0.36$ and $B_H/G_H = 3.19$ at 14 GPa. In the case of the shear anisotropy factor A it is found that for $\phi_\kappa = 3.72°$, A decreases reaching a minimum value 1.68 at 10.7 GPa and above that pressure it increases with pressure reaching a value of 1.83 at 20 GPa. In this respect, we want to stress that the change of the pressure coefficient of the theoretically calculated G and E elastic moduli at HP seems to be related to the mechanical instability of the DC structure above 13.8 GPa. A similar result was found for $HgGa_2Se_4$[33]. Therefore, these behaviors could be related to the onset of the cation-vacancy disorder process and evidenced by the appearing of dark linear defects visually observed in HP measurements as already commented, thus suggesting that the appearance of dark linear defects could be related to the mechanical instability. In this respect, more experimental and theoretical work is needed to confirm whether this fact is a general trend in other DC compounds and in general in adamantine OVCs.

5. Conclusions

We have performed XRD measurements at room temperature in defect chalcopyrite $HgGa_2S_4$ at high pressures and have compared the results with *ab initio* total energy calculations. Experiments show that the pressure dependence of the volume, lattice parameters, and axial ratio of DC-$HgGa_2S_4$ is similar to that of other AGa_2X_4 (A = Mn, Zn, Cd, Hg; X = S, Se) adamantine OVCs. The evolution with pressure of the internal cation–anion and vacancy-anion distances is given showing that the vacancy-S distance is the most compressible one.

Additionally, a theoretical study of the elastic properties of DC-$HgGa_2S_4$ at different pressures has been accomplished. At RP the elastic constants and elastic moduli obtained for the tetragonal phase are in agreement with other calculations for similar compounds of the AGa_2X_4 family. From those results it can be observed that the elastic moduli of sulfides are slightly larger than those of the corresponding selenides. Furthermore, the evolution of the elastic constants with pressure has been reported for future comparison with experimental measurements. From those results we have performed a study of the mechanical stability of the tetragonal phase at high pressures and found that the tetragonal DC-$HgGa_2S_4$ crystal becomes mechanically unstable at pressures above 13.8 GPa.

Acknowledgements

This study was supported by the Spanish government MEC under Grants No: MAT2010-21270-C04-01/03/04 and CTQ2009-14596-C02-01, by the Comunidad de Madrid and European Social Fund (S2009/PPQ-1551 4161893), by MALTA Consolider Ingenio 2010 Project (CSD2007-00045), by Generalitat Valenciana (GVA-ACOMP-2013-1012), and by the Vicerrectorado de Investigación y Desarrollo of the Universidad Politécnica de Valencia (UPV2011-0914 PAID-05-11 and UPV2011-0966 PAID-06-11). E.P-G., A.M., and P.R-H. acknowledge computing time provided by Red Española de Supercomputación (RES) and MALTA-Cluster. J.A.S. acknowledges Juan de la Cierva fellowship program for financial support.

References

[1] H. Hahn, G. Frank, W. Klinger, A. Störger, G. Störger, Z. Anorg, Allg. Chem. 279 (1955) 241.
[2] H. Schwer, V. Krämer, Z Kristallogr. 190 (1990) 103.
[3] V.V. Atuchin, V.G. Kesler, V.V. Ursaki, V.E. Tezlevan, Solid State Commun. 138 (2006) 250.
[4] A. MacKinnon, Tables of numerical data and functional relationships in science and technology, in: O. Madelung, M. Schulz, H. Weiss (Eds.), Landolt–Börnstein New Series, Group III, vol. 17, Springer-Verlag, Berlin, 1985, p. 124 (pt. h).
[5] A.N. Georgobiani, S.I. Radautsan, I.M. Tiginyanu, Sov. Phys. Semicond. 19 (1985) 121.
[6] J.E. Bernard, A. Zunger, Phys. Rev. B 37 (1988) 6835.
[7] X. Jiang, W.R.L. Lambrecht, Phys. Rev. B 69 (2004) 035201.
[8] B.F. Levine, C.G. Bethea, H.M. Kasper, F.A. Thiel, IEEE J. Quantum Electron. QE-12 (1976) 367.
[9] V.V. Ursaki, P.C. Ricci, I. Tiginyanu, A. Anedda, N.N. Syrbu, V.E. Tezlevan, J. Phys. Chem. Solids 63 (2002) 1823.
[10] F. Rotermund, V. Petrov, Opt. Lett. 25 (2000) 746.
[11] V.V. Badikov, N.V. Kuzmin, V.B. Laptev, A.L. Malinovsky, K.V. Mitin, G.S. Nazarov, E.A. Ryabov, A.M. Seryogin, N.I. Shchebetova, Quantum Electron. 34 (2004) 451.
[12] F. Rotermund, V. Petrov, F. Noack, Opt. Commun. 185 (2000) 177.
[13] I.I. Burlakov, Y. Raptis, V.V. Ursaki, E. Anastassakis, I.M. Tiginyanu, Solid State Commun. 101 (1997) 377.
[14] J. González, R. Rico, E. Calderón, M. Quintero, M. Morocoima, Phys. State Solid (b) 211 (1999) 45.
[15] V.V. Ursaki, I.I. Burlakov, I.M. Tiginyanu, Y.S. Raptis, E. Anastassakis, A. Anedda, Phys. Rev. B 59 (1999) 257.
[16] M. Fuentes-Cabrera, O.F. Sankey, J. Phys.: Condens. Matter 13 (2001) 1669.
[17] M. Fuentes-Cabrera, J. Phys.: Condens. Matter 13 (2001) 10117.
[18] A. Grzechnik, V.V. Ursaki, K. Syassen, I. Loa, I.M. Tiginyanu, M. Handfland, J. Solid State Chem. 160 (2001) 205.
[19] T. Mitani, S. Onari, K. Allakhverdiev, F. Gashimzade, T. Kerimova, Phys. State Solid (b) 223 (2001) 287.
[20] A. Tatsi, D. Lampakis, E. Liarokapis, S.A. López, L. Martínez, W. Giriat, High Press. Res. 22 (2002) 89.
[21] I.M. Tiginyanu, V.V. Ursaki, F.J. Manjón, V.E. Tezlevan, J. Phys. Chem. Solids 64 (2003) 1603.
[22] T. Mitani, T. Naitou, K. Matsuishi, S. Onari, K. Allakhverdiev, F. Gashimzade, T. Kerimova, Phys. State Solid (b) 235 (2003) 321.
[23] K. Allakhverdiev, F. Gashimzade, T. Kerimova, T. Mitani, T. Naitou, K. Matsuishi, S. Onari, J. Phys. Chem. Solids 64 (2003) 1597.
[24] J. Marquina, Ch. Power, P. Grima, M. Morocoima, M. Quintero, B. couzinet, J.C. Chervin, P. Munsch, J. González, J. Appl. Phys. 100 (2006) 093513.
[25] S. Meenakshi, V. Vijyakumar, B.K. Godwal, A. Eifler, I. Orgzall, S. Tkachev, H.D. Hochheimer, J. Phys. Chem. Solids 67 (2006) 1660.
[26] D. Errandonea, R.S. Kumar, F.J. Manjón, V.V. Ursaki, I.M. Tiginyanu, J. Appl. Phys. 104 (2008) 063524.
[27] S. Meenakshi, V. Vijyakumar, A. Eifler, H.D. Hochheimer, J. Phys. Chem. Solids 71 (2010) 832.
[28] P. Singh, M. Sharma, U.P. Verma, P. Jensen, Z. Kristallogr. 225 (2010) 508.
[29] F.J. Manjón, O. Gomis, P. Rodríguez-Hernández, E. Pérez-González, A. Muñoz, D. Errandonea, J. Ruiz-Fuertes, A. Segura, M. Fuentes-Cabrera, I. Tiginyanu, V.V. Ursaki, Phys. Rev. B 81 (2010) 195201.
[30] U.P. Verma, P. Singh, P. Jensen, Phys. Status Solidi (b) 248 (2011) 1682.
[31] O. Gomis, R. Vilaplana, F.J. Manjón, E. Pérez-González, J. López-Solano, P. Rodríguez-Hernández, A. Muñoz, D. Errandonea, J. Ruiz-Fuertes, A. Segura, D. Santamaría-Pérez, I.M. Tiginyanu, V.V. Ursaki, J. Appl. Phys. 111 (2012) 013518.
[32] O. Gomis, R. Vilaplana, F.J. Manjón, D. Santamaría-Pérez, D. Errandonea, E. Pérez-González, J. López-Solano, P. Rodríguez-Hernández, A. Muñoz, I.M. Tiginyanu, V.V. Ursaki, Mat. Res. Bull. 48 (2013) 2128.
[33] O. Gomis, R. Vilaplana, F.J. Manjón, D. Santamaría-Pérez, D. Errandonea, E. Pérez-González, J. López-Solano, P. Rodríguez-Hernández, A. Muñoz, I.M. Tiginyanu, V.V. Ursaki, J. Appl. Phys. 113 (2013) 073510.
[34] R. Vilaplana, M. Robledillo, O. Gomis, J.A. Sans, F.J. Manjón, E. Pérez-González, P. Rodríguez-Hernández, A. Muñoz, I.M. Tiginyanu, V.V. Ursaki, J. Appl. Phys. 113 (2013) 093512.
[35] I.M. Tiginyanu, N.A. Modovyan, O.D. Stoika, Fiz. Tverd. Tela 34 (1992) 967; I.M. Tiginyanu, N.A. Modovyan, O.D. Stoika, Idem, Sov. Phys. Solid State 43 (1992) 527.
[36] D. Santamaría-Pérez, A. Vegas, C. Muehle, M. Jansen, Acta Cryst. B 67 (2011) 109.
[37] D. Santamaría-Pérez, M. Marqués, R. Chuliá-Jordán, J.M. Menéndez, O. Gomis, J. Ruiz-Fuertes, J.A. Sans, D. Errandonea, J.M. Recio, Inorg. Chem. 51 (2012) 5289.
[38] S. Klotz, J.C. Chervin, P. Munsch, G. Le Marchand, J. Phys. D: Appl. Phys. 42 (2009) 075413.
[39] D. Errandonea, Y. Meng, M. Somayazulu, D. Häusermann, Phys. B 355 (2005) 116.
[40] H.K. Mao, J. Xu, P.M. Bell, J. Geophys. Res. 91 (1986) 4673.
[41] D. Errandonea, R. Boehler, S. Japel, M. Mezouar, L.R. Benedetti, Phys. Rev. B 73 (2006) 092106.
[42] Oxford Diffraction, CrysAlis, Oxford Diffraction Ltd, Abingdon, England, 2006.
[43] J. Laugier, B. Bochu, <http://www.ccp14.ac.uk/tutorial/lmgp/>.
[44] W. Kraus, G. Nolze, J. Appl. Crystallogr. 29 (1996) 301.
[45] A.C. Larson, R.B. von Dreele, LANL, Report 86-748, 2004.
[46] B.H. Toby, J. Appl. Cryst. 34 (2001) 210.
[47] G. Kresse, J. Hafner, Phys. Rev. B 47 (1993) 558; G. Kresse, J. Hafner, Phys. Rev. B 49 (1994) 14251; G. Kresse, J. Furthmüller, Comput. Mater. Sci. 6 (1996) 15; G. Kresse, J. Furthmüller, Phys. Rev. B 54 (1996) 11169.
[48] J.P. Perdew, A. Ruzsinszky, G.I. Csonka, O.A. Vydrov, G.E. Scuseria, L.A. Constantin, X. Zhou, K. Burke, Phys. Rev. Lett. 100 (2008) 136406.
[49] A. Mujica, A. Rubio, A. Muñoz, R.J. Needs, Rev. Mod. Phys. 75 (2003) 863.
[50] N. Chetty, A. Muñoz, R.M. Martin, Phys. Rev. B 40 (1989) 11934.
[51] S. Baroni, S. de Gironcoli, A. Dal Corso, P. Giannozzi, Rev. Mod. Phys. 73 (2001) 515.
[52] Y. Le Page, P. Saxe, Phys. Rev. B 65 (2002) 104104.
[53] O. Beckstein, J.E. Klepeis, G.L.W. Hart, O. Pankratov, Phys. Rev. B 63 (2001) 134112.
[54] J.F. Nye, Physical properties of crystals, in: Their Representation by Tensor and Matrices, Oxford University Press, 1957.
[55] E. Bandiello, D. Errandonea, D. Martinez-Garcia, D. Santamaria-Perez, F.J. Manjon, Phys. Rev. B 85 (2012) 024108.
[56] M.D. Frogley, J.L. Sly, D.J. Dunstan, Phys. Rev. B 58 (1998) 12579.
[57] F. Birch, J. Geophys. Res. 83 (1978) 1257.
[58] R.J. Angel, Equations of state, in: R.M. Hazen, R.T. Downs (Eds.), High-Pressure and High-Temperature Crystal Chemistry, 41, MSA Reviews in Mineralogy and Geochemistry, 2000, pp. 35–60.
[59] R.J. Angel, J.L. Mosenfelder, C.S.J. Shaw, Phys. Earth Planet Inter. 124 (2001) 71.
[60] L. Garbato, F. Ledda, A. Rucci, Prog. Cryst. Growth Charact. 15 (1987) 1.
[61] L. Gastaldi, M.G. Simeone, S. Viticoli, Solid State Commun. 55 (1985) 605.
[62] A.G. Khatkevich, Sov. Phys. Crystallogr. 6 (1962) 561.
[63] J.M. Farley, G.A. Saunders, D.Y. Chung, J. Phys. C: Solid State Phys. 6 (1973) 2010.
[64] J.M. Farley, G.A. Saunders, J. Phys. C: Solid State Phys. 5 (1972) 3021.
[65] S.-H. Ma, Z.-Y. Jiao, X.-Z. Zhang, J. Mater. Sci. 47 (2012) 3849.
[66] A. Reuss, Z. Angew, Math. Mech. 9 (1929) 49.
[67] W. Voigt, Lehrbuch der Kristallphysik, Teubner, Leipzig, 1928.
[68] R. Hill, Phys. Soc. London, A 65 (1952) 349.
[69] S.F. Pugh, Philos. Mag. 45 (1954) 823.
[70] V. Tvergaard, J.W. Hutchinson, J. Am. Ceram. Soc. 71 (1988) 157.
[71] K. Lau, A.K. McCurdy, Phys. Rev. B 58 (1998) 8980.
[72] G. Grimvall, B. Magyari-Köpe, V. Ozoliņš, K.A. Persson, Rev. Mod. Phys. 84 (2012) 945.